e-ISSN: 2550-164X

Available online at
https://jmeche.uitm.edu.my/browse-journals/regular-issue/regular-issue-2025-vol-22-3/

Journal of Mechanical Engineering 22(3) 2025, 76 – 94.

Journal of Mechanical Engineering

Predicting Vibration Characteristics of a Bolted Pipe Assembly with Complex Boundary and Interface constraints via the Frequency Based Substructuring Method

Mohamad Affendi Sudin[1], Muhammad Syafiq Aiman Mohd Kahar[1], Andreas Kyprianou[2], Wan Imaan Izhan Wan Iskandar Mirza[1], Mohd Azmi Yunus[1], Rina Febrina[3], Rajasekhara Reddy Mutra[4], and Muhamad Norhisham Abdul Rani[1]*

[1]*Structural Dynamics Analysis & Validation (SDAV), Faculty of Mechanical Engineering, Universiti Teknologi MARA (UiTM), Shah Alam, Selangor, Malaysia.*
[2]*Department of Mechanical and Manufacturing Engineering, School of Engineering, University of Cyprus, Nicosia, Cyprus.*
[3]*Civil Engineering Department, Malahayati University, Lampung, 35153, Indonesia.*
[4]*Department Department of Design and Automation, School of Mechanical Engineering, VIT University, Vellore, Tamil Nadu, India.*

ARTICLE INFO

Article history:
Received 25 March 2025
Revised 07 May 2025
Accepted 13 May 2025
Online first
Published 15 September 2025

Keywords:
Vibration characteristics
Bolted joints
Boundary constraints
Experimental modal analysis
Frequency based substructuring

DOI:
https://doi.org/10.24191/jmeche.v22i3.5782

ABSTRACT

Accurately coupling Finite Element Frequency Response Functions (FE-FRFs) with Experimental Modal Analysis Frequency Response Functions (EMA-FRFs) reduces analytical modelling complexity and improves the accuracy of vibration characteristic predictions for complex structures. However, coupling these two different resources remains a major challenge due to complex boundary constraints and bolted joints, which are common in aerospace, automotive, and civil engineering applications. To address these challenges, this study proposes a methodology that integrates the Finite Element Method (FEM), Experimental Modal Analysis (EMA), and Frequency-Based Substructuring (FBS) for accurate and systematic coupling of FE and EMA FRFs. The methodology is demonstrated using a Bolted Flanged Pipe Assembly (BFPA), consisting of a Flanged Elbow Pipe (FEP) and a Flanged Pipe (FP) as a case study. The FE model of the FP substructure is carefully constructed to include coupling interfaces, and its FRFs are computed under free-free boundary constraints. Meanwhile, the FRFs of the FEP substructure, which is extremely difficult to model analytically, are measured using EMA under fixed-free boundary constraints. To achieve accurate coupling, formulations based on the FBS method are developed to integrate FRFs from these two different sources, enabling the prediction of the coupled FRF of the BFPA. Furthermore, EMA is performed on the BFPA to measure its FRFs, which serve as a benchmark. The reliability of the proposed methodology is evaluated by

[1]* Corresponding author. *E-mail address*: mnarani@uitm.edu.my
https://doi.org/10.24191/jmeche.v22i3.5782

the EMA benchmark. The results confirm that the methodology effectively and accurately represents the measured FRF. Its potential applications include accelerated product development, enhanced performance, and improved safety, benefiting industries that rely on precise structural modelling.

INTRODUCTION

It is commonly acknowledged that a system, usually comprising multiple substructures begins to oscillate when subjected to external excitation. This condition worsens when the excitation approaches or corresponds to the natural frequency of the system. This phenomenon is known as resonance. It can lead to unwanted vibrations that shorten the life of the system and, in the worst case, lead to catastrophic situations (Allemang & Avitabile, 2017). Therefore, a thorough understanding of the vibration characteristics of the system is crucial, especially in the design phase, to mitigate adverse vibration effects.

To understand the vibration characteristics of a system, engineers commonly use FEM and EMA (Ewins, 2000). A FE model of the system is constructed, and its accuracy is evaluated with EMA before performing subsequent analyses. However, studies have reported that significant discrepancies often exist between the predicted and measured results (Friswell & Mottershead, 1995; Maia & Silva, 1997; Mohd Kahar et al., 2024; Yu et al., 2021). These discrepancies primarily arise from the limitations of the FE models in accurately representing the physical test system, particularly in accurately modelling boundary conditions (Kreutz et al., 2023; Labbaci et al., 2008; Wang & Yang, 2011) and damping (Caughey, 1960; Crandall, 1970; Mathis et al., 2020). To improve the accuracy of the FE models, engineers commonly adopt FE updating. However, not all case studies have been successfully resolved, particularly for systems with bolted joints (Ibrahim & Pettit, 2005; Mirza et al., 2019; Shi et al., 2024; Sulaiman et al., 2017; Yunus et al., 2017; Zhang et al., 2024). One of the primary challenges is that these substructures are connected through mechanical fasteners such as bolted, welded and riveted joints, which critically influence the vibration characteristics of the system and are particularly difficult to represent numerically with high accuracy. One approach to addressing these challenges is the FBS method.

The FBS method offers a flexible approach, as it allows experimentally derived and analytically derived FRFs to be coupled for investigating the vibration characteristics of a complete assembled system (Allen et al., 2020). In other words, for example, a system composed of two substructures can be independently investigated. One is investigated using EMA and the other one using FEM. The FRF measured through EMA can then be coupled with the FRF calculated from the FE model to form a coupled FRF that represents the complete assembled system. The main advantage of the FBS method can be further noticed in these two scenarios. Firstly, it is very difficult to analytically develop the interfaces between the substructures and the joints (Allen et al., 2020; Liu et al., 2016; Sah et al., 2018). Even in cases where such analytical models can be developed, they are predominantly unreliable and inaccurate, leading to large uncertainties in dynamic predictions. Secondly, in practice, only certain substructures need to be modified or replaced to improve the overall performance and safety of the system (Brøns et al., 2025; Mirza et al., 2024). For example, certain components need to be modified or replaced by new, more powerful ones. This selective modification and replacement make it necessary to accurately model and predict the effects of local changes on global system dynamics, which is difficult to do using conventional methods.

Conventional methods like Finite Element Analysis (FEA) cannot handle those complexities due to nonlinearities (Breunung & Balachandran, 2025; Chen et al., 2022; Jin et al., 2022; Kerschen et al., 2006), uncertainty in damping (Al-hababi et al., 2020; Crandall, 1970; Mathis et al., 2020; Prandina et al., 2009) and coupling effects caused by mechanical joints (Guo et al., 2012; Ibrahim & Pettit, 2005; Li et al., 2021). EMA is a robust and accurate method for measuring the dynamic parameters of a system. However, its applicability is inevitably limited to a fixed configuration of the system design. Since EMA depends on

https://doi.org/10.24191/jmeche.v22i3.5782

testing a physical prototype, proposed changes to the system that could improve performance, such as changes to geometry, material properties, boundary conditions or substructure replacement require the construction of a second prototype and retesting. This scenario renders EMA impractical and uneconomical for iterative design processes where changes are repeatedly evaluated before final realisation.

The coupling of experimental and analytical models through the FBS method offers a promising route for predicting the vibration characteristics of complex mechanical systems. Although FBS has shown exceptional performance and success in academic studies, its practical adoption, especially when coupling EMA and FE models for joint-dominated structures, remains insufficiently explored and validated. It is worth noting that existing literature reviews offer limited information and guidance on adopting FBS to structures with complicated joint configurations and boundary conditions, such as the Bolted Flanged Pipe Assembly (BFPA). The accuracy and robustness of the FBS approach appear to be highly case-dependent, so extensive research is required to establish generalised, reliable methodologies. Therefore, the research gap lies in the lack of a validated and generalised FBS based coupling framework that effectively and accurately couples EMA and FE models for complex jointed structures, which is crucial for engineers to confidently adopt FBS in real-world engineering applications.

This study addresses these challenges by proposing a robust coupling methodology based on the FBS method for coupling EMA and FE models. Despite this advancement, accurately coupling these models remains a considerable challenge, requiring comprehensive and methodical experimental and analytical investigation. By focusing on the BFPA case, this study aims to bridge the identified research gap by proposing an accurate and systematic coupling methodology validated with experimental results. The proposed methodology is expected to provide a robust and accurate methodology that addresses the limitations in the existing research in the area by making a synergy between computational and experimental approach to study the vibration characteristics of bolted structures.

METHODOLOGY

This section describes the detailed methodology and procedures adopted for both FE and EMA investigations to ensure consistency with the main objective of the research stated in the introduction section. The methodology includes EMA, the FE method and the FBS method, which are systematically and carefully integrated to analyse the vibration characteristics of the investigated structure.

This study investigates the vibration characteristics of the BFPA consisting of two substructures: a Flanged Elbow Pipe (FEP) and a Flanged Pipe (FP) connected by bolted joints. The structure is analysed both experimentally and numerically to gain a detailed understanding of its vibration characteristics.

Experimental Modal Analysis

Measurement of BFPA FRFs

Fig 1(a) shows the EMA setup for the measurement of the FRFs. To conduct the measurements, BFPA was securely mounted to the test rig with 18 mm bolted joints at the base plate to represent complex boundary conditions. A reference accelerometer was mounted at a predetermined point on BFPA, serving as the excitation point for all measurement points. In this case, measurement point 39 was chosen because it allowed all modes of interest to be measured. Twelve accelerometers were attached one after the other at different measuring points to measure the FRFs of BFPA. A total of 60 measurement points was used, requiring five measurement runs with 12 accelerometers per run to complete the FRF measurements. Fig 1(b) shows the schematic diagram, and the measuring points used in the measurement of the BFPA FRFs. To minimise uncertainties in FRF measurements, auto-calibration errors, real-time monitoring of coherence, overload detection and time signal were used during testing to identify noise and signal issues

https://doi.org/10.24191/jmeche.v22i3.5782

at early stage. Furthermore, appropriate windowing and exponential averaging were applied to suppress leakage and noise, and H1 estimators were used for FRF computation under clean excitation conditions.

In the FRF measurements, the structure was excited at measurement point 39 (Fig. 1(a)) using the impact testing technique. Each hammer strike provided an input force that excited the vibrational modes of the BFPA, and the force was recorded via the hammer transducer. The vibration responses at the measurement points were captured by the accelerometers, and these signals, along with the input force, were sent to an LMS SCADAS data acquisition system. The recorded time-domain data were processed to compute FRFs, which described the vibration characteristics of the BFPA as a function of frequency. All signals were referenced to the fixed accelerometer to maintain consistency across measurements.

The FRFs were analysed using LMS Test. Lab software to determine the modal parameters of BPFA. The built-in curve-fitting techniques were applied to the FRFs to identify these parameters. The mode shapes were visualized, and the results were evaluated by comparing them with expected values or simulation outputs. This process enabled a detailed understanding of the vibration characteristics of the BPFA, providing valuable insights into its structural behaviour under dynamic loading conditions. Fig. 2 presents the schematic diagram of the measurements of the BFPA FRFs.

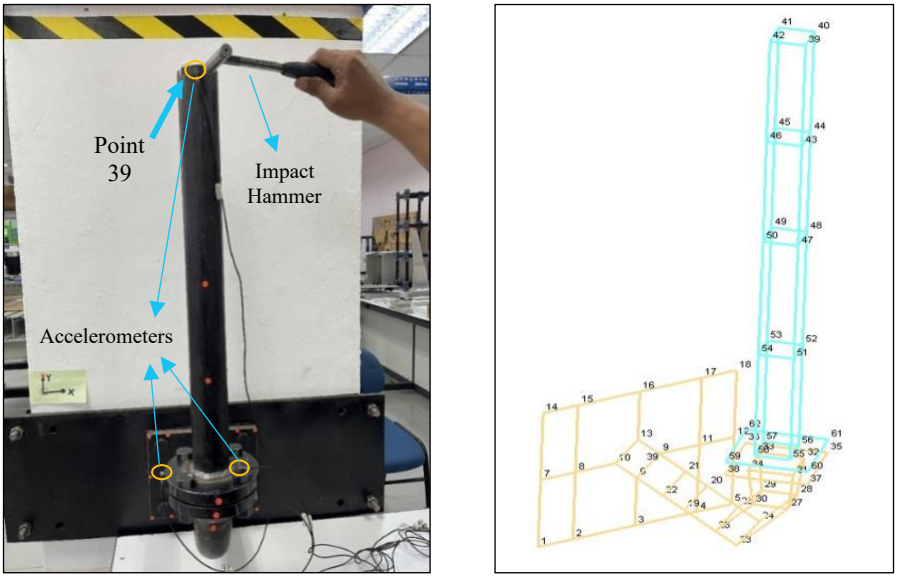

Fig. 1. (a) The detailed EMA set-up of BFPA; (b) schematic diagram and the measurement points of the BFPA FRFs.

Measurement of FEP FRFs

To accurately measure the FRFs of FEP, EMA was carefully set up (Fig. 3(a)) and performed. This included a precise setup to measure the FRFs in all three spatial directions (X, Y, Z) at measuring points 35, 36, 37 and 38, as shown in Fig. 3(b). Four specially designed jigs were attached to the flange, with each jig holding three accelerometers aligned along the orthogonal axes. This configuration allowed a comprehensive acquisition of the FRFs of FEP and facilitates accurate determination of its modal parameters.

Fig. 4 presents the detailed schematic of the FRF measurement setup for FEP. For accurate acquisition of FRFs during the measurements, impact tests were systematically performed by exciting each surface of

https://doi.org/10.24191/jmeche.v22i3.5782

the jigs ten times. The resulting responses were recorded by 12 accelerometers attached to the jigs, generating 12 FRF data sets per excitation cycle. This rigorous procedure provided a total of 144 FRF data sets, ensuring both statistical reliability and a comprehensive data set for analysis. In addition, the robust bolted connection that secured the FEP to the concrete column ensured precise boundary conditions throughout the testing process, increasing the accuracy of the results. Table 1 provides detailed information on the accelerometers used in this study.

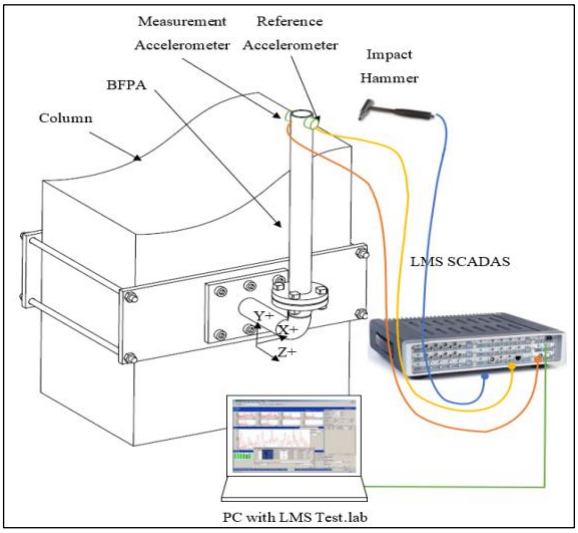

Fig. 2. Schematic diagram and EMA of BFPA.

The dynamic excitation from the impact testing provided input data for the generation of the FRFs, which were analysed to extract the FRFs of FEP. The collected data was processed with a data acquisition system, and the extracted FRFs allowed accurate identification of the vibration characteristics of the structure. This setup was crucial for the coupling of FRFs in the FBS method. The frequency range used in the measurements was from 0 to 1000 Hz.

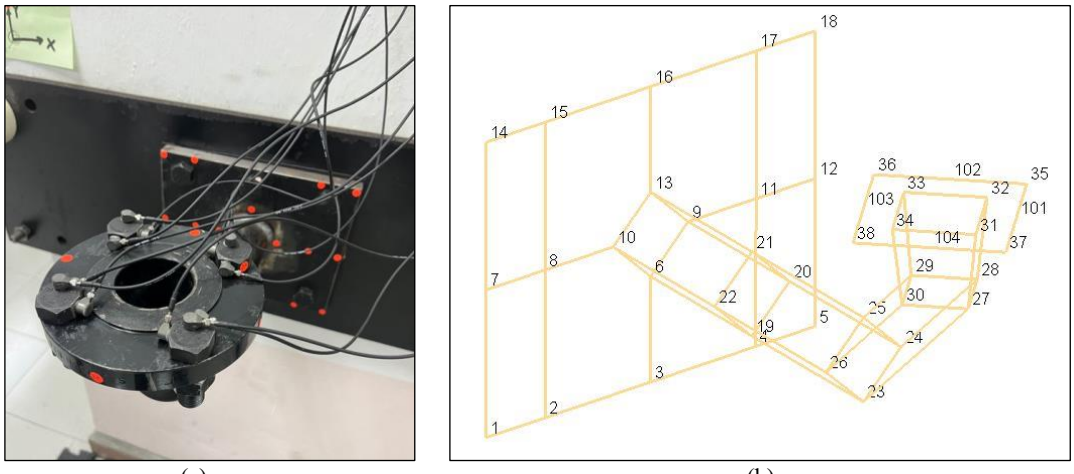

(a) (b)

Fig. 3. (a) The detailed EMA set-up of FEP; (b) schematic diagram and the measurement points of the FEP FRFs.
https://doi.org/10.24191/jmeche.v22i3.5782

Table 1. Information on the accelerometers used in EMA

Apparatus	Manufacturer	Sensitivity	Direction
Accelerometer 1	MMF	10,203 mV/g	X-direction
Accelerometer 2	MMF	10,504 mV/g	Y-direction
Accelerometer 3	MMF	10,307 mV/g	Z-direction

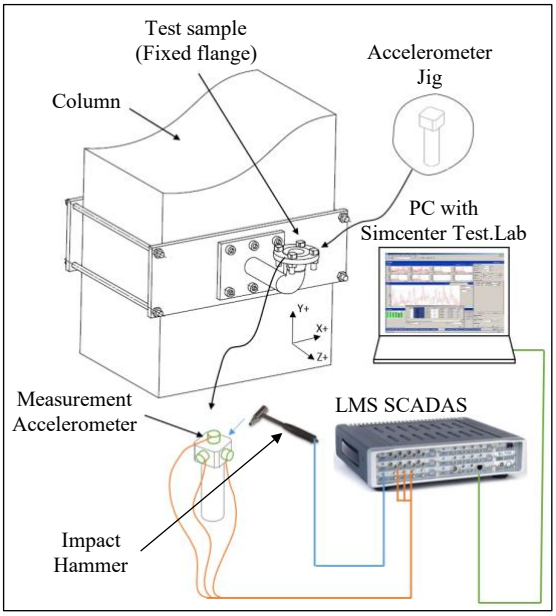

Fig. 4. Schematic diagram and EMA of FEP.

Analytical Simulations

In this subsection, a detailed description of the FE models of the FP and FEP substructures and the BFPA are presented. This is followed by the descriptions of the assembly of both substructures to form the BFPA and of the calculation of FRFs using NASTRAN SOL111 for the substructures and the BFPA.

FE modelling of BFPA under free-free boundary constraints

The FE models of the FP and BEP substructures were created in Hypermesh. The FE model of BFPA consisting of the FP and FEP substructures is shown in Fig 5(a). The model has 122372 CTETRA elements with 32439 nodes and 520 RBE2 (Rigid Body Element, form 2) elements to model the bolted joints between the two flanges (Fig 5(b)). The material properties of the subframe model are tabulated in Table 2.

RBE2 elements were employed to model the bolted joints over CBUSH elements in this study to enforce kinematic compatibility between substructures within the FBS framework. These elements ensure that the interface DOFs are consistently coupled across the coupled structure, which is crucial for the accuracy of dynamic substructuring. In particular, RBE2 elements simplify the enforcement of interface boundary conditions and facilitates modal component coupling by maintaining a consistent transformation of motion between interface DOFs. Therefore, RBE2 elements were considered both sufficient and appropriate in this study, as the chief objective of this study was to predict the global vibration characteristics, which is the FRF of the jointed structure rather than resolving local joint flexibility or interface contact behaviour.

https://doi.org/10.24191/jmeche.v22i3.5782

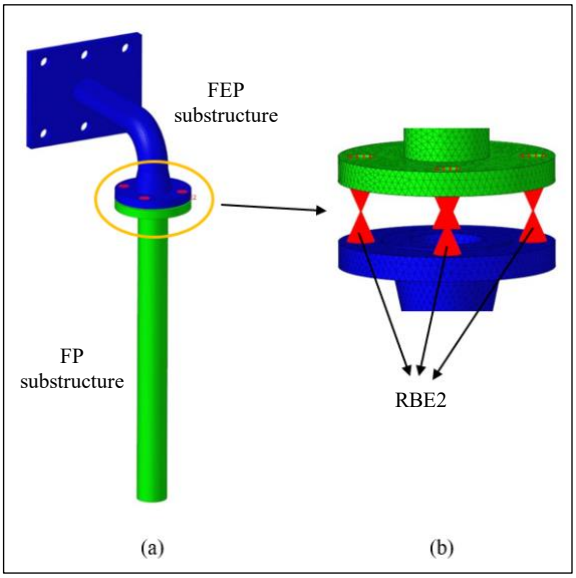

Fig. 5. (a) FE model of the BFPA consisting of FEP and FP substructures; (b) RBE2 elements to represent bolted joints.

Table 2. Material properties of BFPA

Property	Nominal value	Unit
Young's modulus	210	GPa
Poisson's ratio	0.3	Unitless
Mass density	7.89 × 10-6	kg/mm^3

FE modelling of BFPA under fixed-free boundary constraints

The detailed modelling of BFPA was presented in the previous subsection and this subsection presents the fixed-free boundary constraints that were applied to the FE model of BFPA. The FE model was then used as the baseline model for modelling the BFPA with fixed-free boundary constraints (Fig. 6).

In this study, to analytically reproduce fixed-free boundary constraints of the actual test structure, 426 RBE2 elements and 6 constraints were employed to model the bolted joints anchored to the column. Fig. 6 show the detailed FE modelling of BFPA under fixed-free boundary constraints, including the use of RBE2 to model the interfaces between the bolted joints and the surface hole, as well as how BFPA was anchored to the column.

Coupling of FRFs Using the FBS Method

In this subsection, the FBS method for coupling the FE-FRF of the FP with the EMA-FRF of the FEP is presented and discussed, enabling a detailed investigation of the vibration characteristics of the BFPA via the coupled FRF.

The chief goal of the FBS method is to predict the vibration characteristics of a system comprising several substructures based on the free-interface FRF of the uncoupled substructures. The FRF obtained during the assembly uses the structural dynamic stiffness in the frequency domain defined between the points of the subsystems. These FRFs may be determined analytically or experimentally.

https://doi.org/10.24191/jmeche.v22i3.5782

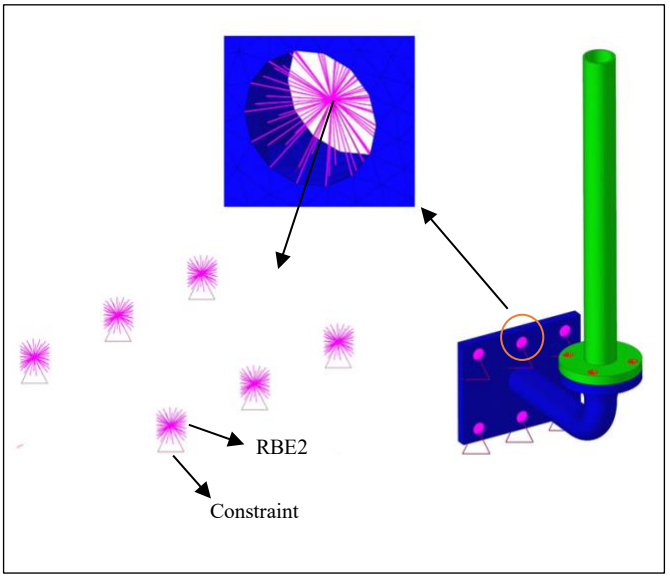

Fig. 6. FE model of the BFPA under fixed-free boundary constraints.

Fundamentals of the FBS method

In this study, the basic theory of the decoupled equations of motion of a substructure *J* in the frequency domain is revisited. The FRF of the substructure can be analytically determined using the dynamic equations of motion in the time domain as follows:

$$\boldsymbol{M}^{J}\ddot{x}(t)^{J}+\boldsymbol{C}^{J}\dot{x}(t)^{J}+\boldsymbol{K}^{J}x(t)^{J}=\boldsymbol{f}(t)^{J} \tag{1}$$

In Equation 1, $\boldsymbol{M}^{J}$, $\boldsymbol{C}^{J}$, and $\boldsymbol{K}^{J}$ denote the matrices of the mass, damping, and stiffness of the substructure. The force excitation vector of the substructure is $\boldsymbol{f}^{J}$.

$$\left[-\omega^{2}\boldsymbol{M}^{J}+j\omega\boldsymbol{C}^{J}+\boldsymbol{K}^{J}\right]\boldsymbol{X}(\omega)^{J}=\boldsymbol{F}(\omega)^{J} \tag{2}$$

By applying a Fourier transform, Equation 1 can be expressed in the frequency domain, which yields

$$\left[-\omega^{2}\boldsymbol{M}^{J}+j\omega\boldsymbol{C}^{J}+\boldsymbol{K}^{J}\right]\boldsymbol{X}(\omega)^{J}=\boldsymbol{F}(\omega)^{J} \tag{3}$$

assigning;

$$\boldsymbol{Z}(\omega)^{J}=\left[-\omega^{2}\boldsymbol{M}^{J}+j\omega\boldsymbol{C}^{J}+\boldsymbol{K}^{J}\right] \tag{4}$$

$$\boldsymbol{H}(\omega)^{J}=\left[\boldsymbol{Z}(\omega)^{J}\right]^{-1} \tag{5}$$

where $\boldsymbol{Z}(\omega)^{J}$ and $\boldsymbol{H}(\omega)^{J}$ represent the Dynamic *Stiffness matrix* of the substructure and its inverse, which is called the *Receptance matrix* of the substructure. Equation 3 can be arranged as follows:

$$\boldsymbol{H}(\omega)^{J}\,\boldsymbol{F}(\omega)^{J}=\boldsymbol{X}(\omega)^{J} \tag{6}$$

https://doi.org/10.24191/jmeche.v22i3.5782

The receptance matrices used in this study to couple the FP and FEP substructures using the FBS method are partitioned based on the work of (Jetmundsen et al., 1988; Klerk et al., 2008; Mahmoudi et al., 2020). However, the notation used in this study has been changed due to the abbreviations used to denote the substructures used in this study. Equations 7 and 8 are the displacements and forces expressed in the receptance matrices of the substructures FP and FEP.

$$\begin{pmatrix} \boldsymbol{X}_A^{FP} \\ \boldsymbol{X}_I^{FP} \end{pmatrix} = \begin{bmatrix} \boldsymbol{H}_{AA}^{FP} & \boldsymbol{H}_{AI}^{FP} \\ \boldsymbol{H}_{IA}^{FP} & \boldsymbol{H}_{II}^{FP} \end{bmatrix} \begin{pmatrix} \boldsymbol{F}_A^{FP} \\ \boldsymbol{F}_I^{FP} \end{pmatrix} \square \left[\boldsymbol{H}\right]^{FP} \begin{pmatrix} \boldsymbol{F}_A^{FP} \\ \boldsymbol{F}_I^{FP} \end{pmatrix} \tag{7}$$

$$\begin{pmatrix} \boldsymbol{X}_B^{FEP} \\ \boldsymbol{X}_I^{FEP} \end{pmatrix} = \begin{bmatrix} \boldsymbol{H}_{BB}^{FEP} & \boldsymbol{H}_{BI}^{FEP} \\ \boldsymbol{H}_{IB}^{FEP} & \boldsymbol{H}_{II}^{FEP} \end{bmatrix} \begin{pmatrix} \boldsymbol{F}_B^{FEP} \\ \boldsymbol{F}_I^{FEP} \end{pmatrix} \square \left[\boldsymbol{H}\right]^{FEP} \begin{pmatrix} \boldsymbol{F}_B^{FEP} \\ \boldsymbol{F}_I^{FEP} \end{pmatrix} \tag{8}$$

The two substructures, FP and FEP, have internal degrees of freedom, which are denoted by the sets *A* and *B,* respectively. The interface shared by the substructures, whose degrees of freedom are represented by *I*. When the two substructures are coupled, they become an assembled structure whose sets of degrees of freedom also contain the degrees of freedom of the interface.

Equations 7 and 8 should follow the coupling conditions, which are the displacement compatibility and force equilibrium:

$$\boldsymbol{X}_I^{FP} + \boldsymbol{X}_I^{FEP} = 0 \tag{9}$$

$$\boldsymbol{F}_I^{FP} + \boldsymbol{F}_I^{FEP} = \Lambda \tag{10}$$

Assembling the receptance equations and coupling conditions of the substructures FP and FEP in a single coupling matrix yields:

$$\begin{bmatrix} \boldsymbol{H}_A^{FP} & 0 & \left(\boldsymbol{C}_I^{FP}\right)^T \\ 0 & \boldsymbol{H}_A^{FEP} & \left(\boldsymbol{C}_I^{FEP}\right)^T \\ \boldsymbol{C}_I^{FP} & \boldsymbol{C}_I^{FEP} & 0 \end{bmatrix} \begin{bmatrix} \boldsymbol{X}_A^{FP} \\ \boldsymbol{X}_A^{FEP} \\ \Lambda_I \end{bmatrix} = \begin{bmatrix} \boldsymbol{F}_A^{FP} \\ \boldsymbol{F}_A^{FEP} \\ 0 \end{bmatrix} \tag{11}$$

Since the assembled structure is referred to as BFPA in this study, the generalised coupled receptance matrix of BFPA is as follows:

$$\begin{aligned} \boldsymbol{H}^{BFPA} = & \begin{bmatrix} \boldsymbol{H}_A^{FP} & 0 \\ 0 & \boldsymbol{H}_A^{FEP} \end{bmatrix} - \begin{bmatrix} \boldsymbol{H}_I^{FP}\left(\boldsymbol{C}_I^{FP}\right)^T & \boldsymbol{H}_I^{FEP}\left(\boldsymbol{C}_I^{FEP}\right)^T \end{bmatrix} \times \\ & \left(\boldsymbol{C}_I^{FP}\boldsymbol{H}_I^{FP}\left(\boldsymbol{C}_I^{FP}\right)^T + \boldsymbol{C}_I^{FEP}\boldsymbol{H}_I^{FEP}\left(\boldsymbol{C}_I^{FEP}\right)^T\right)^{-1} \begin{bmatrix} \boldsymbol{C}_I^{FP}\boldsymbol{H}_I^{FP} \\ \boldsymbol{C}_I^{FEP}\boldsymbol{H}_I^{FEP} \end{bmatrix} \end{aligned} \tag{12}$$

The generalised coupled receptance matrix in Equation 12 can be transformed according to the needs of the investigation. The coupled receptance can be determined from different locations of excitation and measurement.

For example, for the first scenario, excitation is performed at the FP substructure and measurement at the FEP substructure. In the second scenario, excitation and measurement occur at the same location of the substructure, more precisely at the FP substructure

https://doi.org/10.24191/jmeche.v22i3.5782

For the first scenario, Equation 12 can be cast into:

$$\boldsymbol{H}_{ji}^{BFPA} = \left[\boldsymbol{H}_I^{FEP} \left(\boldsymbol{C}_I^{FEP} \right)^T \right] \left[\boldsymbol{C}_I^{FP} \boldsymbol{H}_I^{FP} \left(\boldsymbol{C}_I^{FP} \right)^T + \boldsymbol{C}_I^{FEP} \boldsymbol{H}_I^{FEP} \left(\boldsymbol{C}_I^{FEP} \right)^T \right]^{-1} \left[\boldsymbol{C}_I^{FP} \boldsymbol{H}_I^{FP} \right] \tag{13}$$

For the second scenario, Equation (12) can be expressed as:

$$\boldsymbol{H}_{ji}^{BFPA} = \boldsymbol{H}_{I,(j,i)}^{FP} - \left[\boldsymbol{C}_I^{FP} \boldsymbol{H}_I^{FP} \right] \left[\boldsymbol{C}_I^{FP} \boldsymbol{H}_I^{FP} \left(\boldsymbol{C}_I^{FP} \right)^T + \boldsymbol{C}_I^{FEP} \boldsymbol{H}_I^{FEP} \left(\boldsymbol{C}_I^{FEP} \right)^T \right]^{-1} \left[\boldsymbol{C}_I^{FP} \boldsymbol{H}_I^{FP} \right] \tag{14}$$

It is worth noting that Equations 13 and 14 demonstrate the flexibility and advantages of the FBS method for dealing with two different sources of FRFs and allow the coupled receptance of assembled structure to be conveniently determined. Although both formulations can be used, in this study the experimental and analytical identification of the FRFs of the BFPA is based on Equation 14.

RESULTS AND DISCUSSION

This section focuses on investigating the vibration characteristics of the substructures FP and FEP as well as BFPA based on the FE-FRF, EMA-FRF and FBS-FRF, which were obtained using the proposed methodology. The EMA-derived FRF served as benchmark for evaluating the accuracy of those derived from the FE model and the FBS method. In addition, the FBS approach was used to couple the FRF of the substructures and synthesise the FRF of BFPA to obtain a coupled FRF of BFPA.

The EMA procedure for measuring the FRFs of the FP physical test under free-free boundary settings, the BFP and BFPA physical test under fixed-free constraints were clearly described in the 'Experimental Modal Analysis' subsection. Similarly, the FE model of the FE, BFP and BFPA under the same boundary conditions and the calculations of its FRFs were clearly explained in the 'Analytical Simulations' subsection.

The results of this chapter show and discuss a comparison between the FE-FRFs and EMA-FRFs. Furthermore, the accuracy of the FBS approach in replicating the FRF of BFPA was assessed by benchmarking it against the EMA-FRF. The results were thoroughly evaluated to highlight the strengths and weaknesses of the integrated approach and illustrate the advantages of the approach for the accuracy of predicting the FRFs of BFPA

Analysis of the FP Substructure

The FE model of FP was validated against the EMA model to evaluate discrepancies between the two results. While the validation of EMA-FRFs and FE-FRFs in the study was defined as up to 1000 Hz, the validation of the FE model extended to 2000 Hz, considering both natural frequencies and FRFs. This extended frequency range was deliberately chosen to ensure that the accuracy of the FRFs used for coupling remained satisfactory up to double the range typically examined (Mirza et al., 2016; Ren & Beards, 1995), thereby increasing the reliability of the coupled FRFs in the study.

Table 3 presents a comparison between the EMA and FE natural frequencies and mode shapes between the model under free-free boundary constraints. The natural frequencies and mode shapes, quantified by the MAC analysis, indicate that the FE model provides satisfactory agreement with the EMA results. However, Fig 7, which compares both EMA and FE-derived FRFs, highlights discrepancies in the amplitude of resonance peaks.

https://doi.org/10.24191/jmeche.v22i3.5782

The first five natural frequencies, listed in columns II and III, demonstrate close agreement between EMA and FE, with percentage errors (column IV) ranging from 0.76% to 2.02%. The total error across all modes is 6.45%, which is within an acceptable range for most engineering applications. Additionally, the high MAC values (column V), all exceeding 0.95, indicate that the mode shapes are well correlated, confirming that the FE model reliably reproduces the EMA mode shapes.

Despite the good agreement in modal parameters, Fig 7 depicts significant differences in the FRFs. The FE model predicts the overall resonance frequencies and general trends of the EMA data but fails to accurately predict the amplitudes of the resonance peaks. For instance, at the first resonance near 650 Hz, the FE model underestimates the amplitude of the EMA response. Additionally, at the second resonance near 1500 Hz, while the frequency is closely aligned, the amplitude mismatch is again evident. These discrepancies suggest that while the natural frequencies and corresponding mode shapes are satisfactory, the FE model does not fully replicate the EMA dynamic stiffness and damping properties.

Table 3. Comparison between the FE and EMA natural frequencies of the FP substructure under free-free boundary constraints

I Mode	II EMA (Hz)	III FE (Hz)	IV Error (%) (II-III)/II	V MAC
1	651.99	658.88	1.06	0.98
2	652.58	658.71	0.94	0.95
3	1498.32	1486.96	0.76	0.96
4	1672.92	1644.89	1.68	0.96
5	1679.13	1645.13	2.02	0.96
	Total Error		6.45	

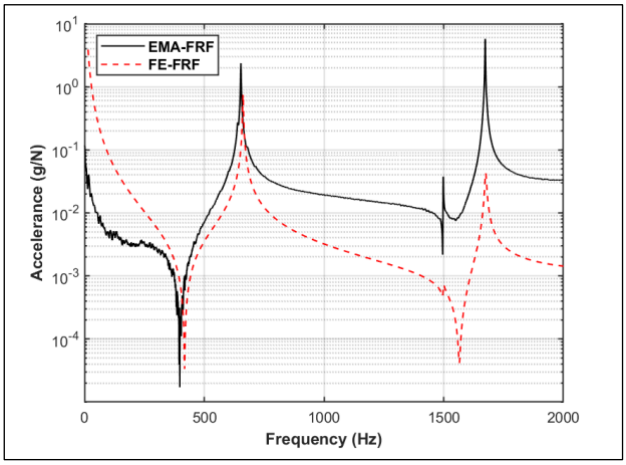

Fig. 7. Comparison between the FE-FRF and EMA-FRF of the FP substructure under free-free boundary constraints.

The inconsistencies in FRF amplitudes indicate that the FE model lacks sufficient accuracy in representing the vibration characteristics of the physical test FP, such as joint dynamics and damping mechanisms arising from the welded joints connecting the flange and the straight pipe are not adequately represented. This limitation is critical because FRFs are directly used in predicting system responses under operational conditions. Therefore, while modal methods provide an initial validation of the FE model, the significant mismatch in FRFs necessitates further refinement of the model to improve its predictive capability.

https://doi.org/10.24191/jmeche.v22i3.5782

Analysis of the FEP Substructure

The FEP substructure under fixed-free boundary constraints

The vibration characteristics of FEP under fixed-free boundary constraints was analysed by comparing the results from the FE model with the EMA-derived results. Table 4 summarises the comparisons of the modal characteristics, while Fig 8 shows the EMA-FRF and FE-FRF of the FEP substructure. This analysis evaluates how accurately the FE model replicates the physical test FP under these boundary conditions.

Table 4 highlights significant discrepancies between the EMA and FE model, particularly in natural frequencies, while demonstrating strong agreement in mode shapes under fixed-free boundary constraints. However, the FE model exhibits low overall agreement with the EMA for most modes and fails to predict the second mode, resulting in an MAC value of 0.00. This outcome suggests that the FE model has limited capability in accurately capturing certain dynamic properties, particularly for lower-order modes.

Table 4. Comparison between the FE and EMA natural frequencies of the FEP substructure under fixed-free boundary constraints

I Mode	II EMA (Hz)	III FE (Hz)	IV Error (%) (II-III)/II	V MAC
1	165.51	176.65	6.86	0.93
2	179.62	Missed Mode	0.00	0.00
3	439.63	567.38	29.06	0.90
4	655.83	654.33	0.23	0.95
5	938.18	1036.32	10.46	0.90
	Total Error		52.27	

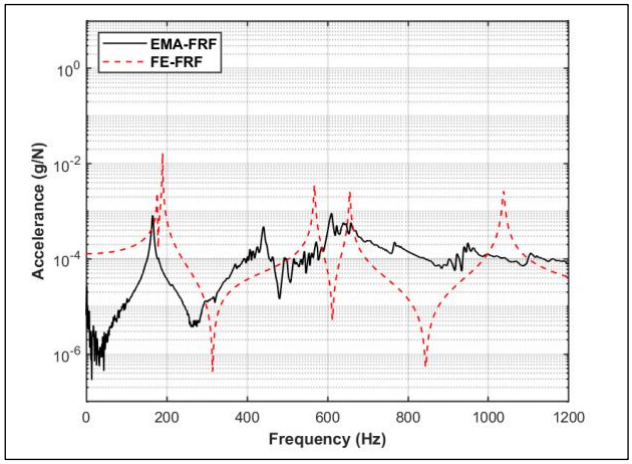

Fig. 8. Comparison between the FE-FRF and EMA-FRF of the FEP substructure under fixed-free boundary constraints.

For the other modes, the total error for all natural frequencies is 52.27 Hz, with individual deviations ranging from approximately 0.23 Hz to 29.06 Hz. The MAC values for the other modes exceed 0.90, highlighting good agreement in terms of mode shapes despite discrepancies in frequencies. However, with the largest error of 29.06 Hz recorded from the third mode shape, these results show inaccuracies in the modelling. These inaccuracies indicate that the FE has limited ability to predict the full spectrum of dynamic properties, especially for lower modes and specific configurations.

https://doi.org/10.24191/jmeche.v22i3.5782

Fig 8 shows significant discrepancies between the EMA-FRF and FE-FRF, particularly in terms of the trends of the resonance peaks and the amplitude. While the overall trends of the FRFs match, the FE model fails to accurately represent certain resonance frequencies and their corresponding amplitudes, particularly in the range of 400 Hz to 600 Hz and beyond. These inconsistencies indicate that the FE model has difficulty accurately representing the effects of boundary conditions, damping mechanisms and other structural dynamics under fixed conditions.

Furthermore, the absence of the second mode and the discrepancies in the FRF clearly show that it is insufficient to rely solely on modal characteristics for validation. Compared to modal validation, FRF-based validation provides a more detailed characterisation of the vibration characteristics and exposes deficiencies that modal validation alone cannot address.

The results of the comparison underline the need for a dual validation approach that integrates both modal and FRF-based analyses to ensure a comprehensive assessment of the accuracy of the FE model. While the MAC values confirm that the FE model predicts the mode shapes well for most modes, the absence of the second mode and the significant frequency errors in the third and fifth modes clearly show critical gaps in the model. These limitations are amplified by the FRF discrepancies, which indicate that the FE representation of damping and boundary conditions needs to be significantly improved.

The limitation in predicting certain modes and accurately reproducing the EMA-FRF shows the need for more advanced refinement techniques. Enhancing the accuracy of the FE model in these areas is critical for reliable performance under different boundary conditions.

Under fixed-free constraints, the FEP substructure analysis confirms that while the FE model accurately predicts mode shapes, its inability to predict natural frequencies accurately highlights critical limitations. Moreover, the absence of the second mode and the large deviations in the FRFs further emphasize critical deficiencies in the predictive capability of the FE model. These comprehensive results emphasise the importance of FRF-based validation as a complement to modal validation to provide a more comprehensive assessment of the FE model and strongly underline the need for other advanced techniques when it comes to analysing structures with complex boundary conditions and interfaces.

Analysis of BFPA via FEM

The ability of FEM in representing complex boundary conditions and interfaces was demonstrated in the previous subsections. It was clearly shown that the FE model of FEP is incapable of accurately representing the complexity of the boundary conditions and interfaces arising from damping mechanisms.

In this subsection, the comprehensive comparisons of the modal parameters and the FRFs obtained from the EMA of the BFPA physical test and the FE model of BFPA under fixed-free boundary conditions are presented and discussed.

BFPA under fixed-free boundary constraints

The EMA procedure for measuring the FRFs of the BFPA under fixed-free boundary constraints was clearly described in the 'Experimental Modal Analysis' subsection. Similarly, the FE model of the BFPA under the same boundary conditions was carefully developed, and the calculation of its FRFs was clearly explained in the 'Analytical Simulations' subsection.

As shown in Table 5, a detailed comparison is provided between the EMA and FE natural frequencies of BFPA for fixed-free boundary constraints. The EMA natural frequencies in Column II, the FE natural frequencies in Column III, the percentage error between them in Column IV, and in Column V the MAC values. In the case of mode 1, the EMA natural frequency is 46.25 Hz, while the FE model predicts it to be 55.11 Hz, resulting in a percentage error of 19.15%. However, the MAC value is 0.98, which shows a strong correlation between the mode shapes determined from the EMA and the FE model. However, the FE model

https://doi.org/10.24191/jmeche.v22i3.5782

does not reflect this as Mode 2 is not predicted (with matching frequency), so the corresponding error and MAC values for this mode are 0.00.

Table 5. Comparison between the FE and EMA natural frequencies of BFPA under free-free boundary constraints

I Mode	II EMA (Hz)	III FE (Hz)	IV Error (%) (II-III)/II	V MAC
1	46.25	55.11	19.15	0.98
2	157.60	Missed	0.00	0.00
3	163.43	193.27	18.25	0.96
4	374.51	424.35	13.30	0.96
5	955.19	975.65	2.14	0.96
	Total Error		52.84	

Mode 3 shows that the EMA natural frequency for this mode is 163.43 Hz, while the FE model predicts 193.27 Hz, which corresponds to an error of 18.25%. The MAC value of 0.96 in this mode indicates a good correlation between the mode shapes. For mode 4, the EMA frequency is 374.51 Hz, while the FE model predicts a value of 424.35 Hz, resulting in a percentage error of 13.30%. The MAC value is consistently high across the entire data set at 0.96. Mode 5 has the smallest difference at 955.19 Hz (EMA frequency) and 975.65 Hz (FE frequency), with a MAC value of 0.96 and an error of only 2.14%.

Consequently, the total error across all modes is 52.84%, indicating that there are significant differences between the FE and EMA predictions. These differences indicate that the FE model performs quite well for the higher modes but has difficulty predicting the lower modes and even omits certain modes altogether.

Fig 9 shows a comprehensive analysis of the EMA-FRF and FE-FRF for BFPA under fixed-free boundary constraints. The comparison covers the range from 0 to 1200 Hz. The EMA-FRF is the solid black line, while the FE-FRF is the dashed red line.

The EMA-FRF and FE-FRF show a similar trend in which the resonance peaks occur at approximately the same frequencies. However, clear discrepancies appear in certain frequency ranges. In particular, the FE model cannot predict the second mode identified in the EMA-FRF, which leads to a gap in the frequency response. For the higher modes, the FE model predicts resonance frequencies reasonably well, although there are discrepancies in the magnitude of the responses near the peaks. This discrepancy indicates that the FE model does not fully account for damping, joint behaviour or other structural nonlinearities present in the physical system.

Analysis of BFPA via FBS

Table 6 and Fig. 10 compare the EMA-FRF and FBS-FRF, clearly demonstrating the strong performance of the FBS method in predicting the actual vibration characteristics of the BFPA. The FBS-FRF closely matches the EMA-FRF across all frequency ranges, confirming that the FBS method effectively reproduces the dynamic characteristics of the physical test BFPA. However, local differences in frequency, amplitude and anti-resonance highlight areas where further adjustments to the FBS method may be necessary. In particular, there are slight discrepancies in resonance frequencies, particularly at 900 Hz and 1400 Hz. These discrepancies suggest that the stiffness or boundary conditions are inaccurately represented in the substructure models used for FBS and emphasise the importance of fine-tuning the substructure parameters to achieve better agreement with the EMA results.

For comparative amplitudes, the FBS-FRF is in good agreement with the EMA-FRF at low frequencies, especially below 500 Hz. But in the mid to high frequency ranges, such as 400-600 Hz and 900-1400 Hz, the FBS-FRF sometimes exceeds the amplitude of the resonances. For example, the peaks at 400 Hz and 900 Hz are more pronounced in the FBS-FRF than in the EMA. These amplitude differences may be due

https://doi.org/10.24191/jmeche.v22i3.5782

to an inaccurate representation of the damping or coupling conditions within the FBS. Since the damping effect at joints and interfaces can differ significantly between experimental and numerical representations, these differences require further investigation.

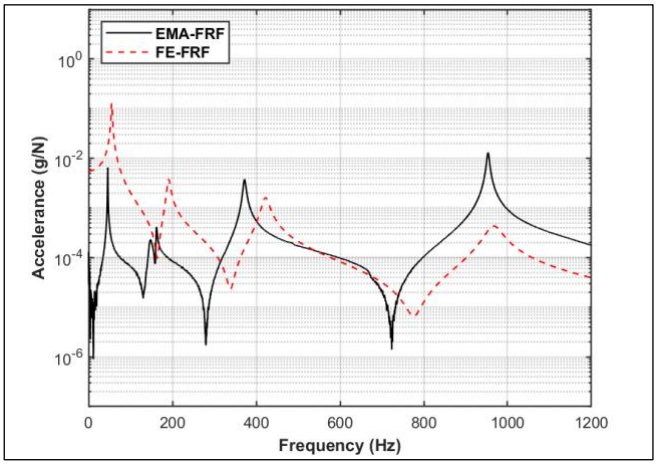

Fig. 9. Comparison between the FE-FRF and EMA-FRF of BFPA under fixed-free boundary constraints.

Most antiresonances are well represented in FBS, but the information between certain frequencies and depths differs somewhat from the experimental antiresonances of mode analysis. For example, at around 1200 Hz the FBS-FRF does not become as low as the corresponding EMA-FRF, which has already dropped below -100 dB, and at around 1400 Hz there is a significant phase shift. Some of these differences in resonance behaviour could indicate ill- conditioning of the substructure coupling used by FBS.

Table 6. Comparison between the FBS and EMA natural frequencies of BFPA under fixed-free boundary constraints

I Mode	II EMA (Hz)	III FE (Hz)	IV Error (%) (II-III)/II	V MAC
1	46.25	47.31	2.29	0.97
2	157.60	159.21	1.02	0.97
3	163.43	165.27	1.13	0.95
4	374.51	376.35	0.49	0.98
5	955.19	883.65	7.48	0.90
6	1423.62	1375.25	3.39	0.91
7	1828.32	1854.65	1.44	0.95
	Total Error		17.23	

Despite these discrepancies in localisation, the overall trend of the FBS-FRF is indeed very close to the EMA-FRF. This overall agreement confirms how well the FBS can be used to predict the fundamental vibration characteristics of BFPA. In contrast, FE-FRF (Fig. 9) shows larger discrepancies in both resonance frequencies and amplitudes, especially around the two frequency peaks: 200 Hz and 1000 Hz, indicating inaccuracies in the representation of stiffness and damping.

Overall, the FBS-FRF appears to be a closer representation of the EMA-FRF than FE-FRF, which fails to show agreement. However, fine-tuning of the FBS model is required to accurately predict the dynamics. Furthermore, these findings highlight the utility and predictive power of FBS, especially in a scenario where: 1) developing analytical models of the substructures is challenging. 2) developing analytical models

https://doi.org/10.24191/jmeche.v22i3.5782

of the substructures is impossible due to the unavailability of design dimensions. 3) direct and reliable experimental results can be successfully obtained.

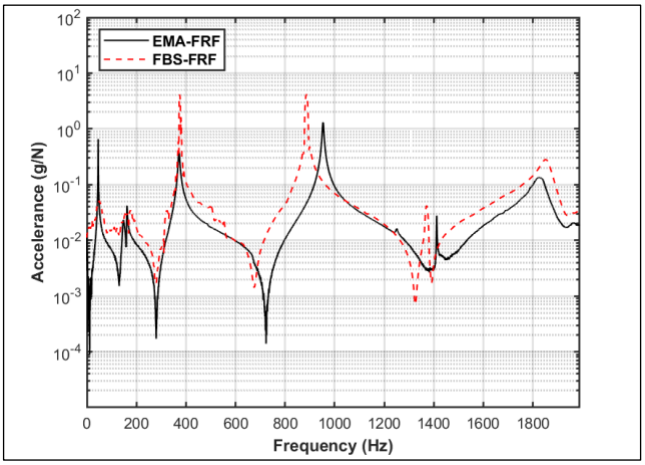

Fig. 10. Comparison between the FBS-FRF and EMA-FRF of BFPA under fixed-free boundary constraints.

CONCLUSIONS

In this study, the performance of FBS and FE in predicting the vibration characteristics of an assembled structure with complex boundary constraints and interfaces, namely BFPA, was evaluated in comparison with the results of EMA. The results emphasise that FBS largely agrees with EMA and is able to satisfactorily predict resonance frequencies and trends similar to EMA performance. The FBS-FRF show consistent trends, but amplitude and frequency shifts, particularly at 400 Hz, 900 Hz and 1400 Hz, emphasise the importance of refining the damping and coupling assumptions of the substructure.

In contrast to the FRF predicted by the BFPA-FE model, which increasingly deviated from the EMA-FRF particularly at resonance frequencies and amplitudes above 200 Hz and 1000 Hz, the matching stiffness and damping, which are very difficult to estimate, were not accurately represented by the FE model. Although the FE model predicted the general trends, it performed poorly compared to the FBS model, once again emphasising the importance of updating the model and tuning the parameters.

This study is subject to certain limitations. The accuracy of the proposed methodology is primarily applicable to linear vibration responses and lower modes. Future work should address the coupling of more complex joints and nonlinear frequency response functions, as well as extend it to higher modes. These advancements would further enhance the proposed methodology to more complex jointed structures.

To summarise, the FBS model performed better than the FE model in representing the results of the EMA model, demonstrating that it is a powerful tool for integrating experimental and computational information to predict complex structural dynamics.

https://doi.org/10.24191/jmeche.v22i3.5782

ACKNOWLEDGEMENTS

This study is supported by Universiti Teknologi MARA (UiTM) through the Strategic Research Partnership (SRP) grant RMC 5/3/SRP (086/2022) and the VIT-International Research Fund Scheme (VIN) under award VIN/2022-23/002. The authors would like to express their gratitude to the members of SDAV UiTM Shah Alam and the Department of Design and Automation, School of Mechanical Engineering, VIT University, Vellore, for their valuable technical support.

CONFLICT OF INTEREST

All authors declare that they have no conflicts of interest.

AUTHORS' CONTRIBUTIONS

The authors confirm the equal contribution in each part of this work. All authors reviewed and approved the final version of this paper.

REFERENCE

Al-hababi, T., Cao, M., Saleh, B., Alkayem, N. F., & Xu, H. (2020). A critical review of nonlinear damping identification in structural dynamics: Methods, applications, and challenges. Sensors, 20(24), 7303.

Allemang, R., & Avitabile, P. (2017). Handbook of experimental structural dynamics. Springer New York.

Allen, M. S., Rixen, D., Van der Seijs, M., Tiso, P., Abrahamsson, T., & Mayes, R. L. (2020). Substructuring in engineering dynamics. Springer Cham.

Breunung, T., & Balachandran, B. (2025). Frequency response based identification of nonlinear oscillators. Journal of Sound and Vibration, 594, 118651.

Brøns, M., Trainotti, F., & Rixen, D. J. (2025). A novel optimization framework using frequency-based substructuring for estimation of linear bolted joint stiffness and damping. Mechanical Systems and Signal Processing, 223, 111806.

Caughey, T. K. (1960). Classical normal modes in damped linear dynamic systems. Journal of Applied Mechanics, 27(2), 269-271.

Chen, W., Jana, D., Singh, A., Jin, M., Cenedese, M., Kosova, G., Brake, M. R. W., Schwingshackl, C. W., Nagarajaiah, S., Moore, K. J., & Noël, J. P. (2022). Measurement and identification of the nonlinear dynamics of a jointed structure using full-field data, Part I: Measurement of nonlinear dynamics. Mechanical Systems and Signal Processing, 166, 108401.

Crandall, S. H. (1970). The role of damping in vibration theory. Journal of Sound and Vibration, 11(1), 3-18.

Ewins, D. J. (2000). Modal testing: Theory, practice and application. Wiley.

Friswell, M. I., & Mottershead, J. E. (1995). Finite element model updating in structural dynamics. Springer

https://doi.org/10.24191/jmeche.v22i3.5782

Dordrecht.

Guo, T., Li, L., Cai, L., & Zhao, Y. (2012). Alternative method for identification of the dynamic properties of bolted joints. Journal of Mechanical Science and Technology, 26(10), 3017-3027.

Ibrahim, R. A., & Pettit, C. L. (2005). Uncertainties and dynamic problems of bolted joints and other fasteners. Journal of Sound and Vibration, 279(3-5), 857-936.

Jetmundsen, B., Bielawa, R. L., & Flannelly, W. G. (1988). Generalized frequency domain substructure synthesis. Journal of the American Helicopter Society, 33(1), 55-64.

Jin, M., Kosova, G., Cenedese, M., Chen, W., Singh, A., Jana, D., Brake, M. R. W., Schwingshackl, C. W., Nagarajaiah, S., Moore, K. J., & Noël, J. P. (2022). Measurement and identification of the nonlinear dynamics of a jointed structure using full-field data; Part II - Nonlinear system identification. Mechanical Systems and Signal Processing, 166, 108402.

Kerschen, G., Worden, K., Vakakis, A. F., & Golinval, J. C. (2006). Past, present and future of nonlinear system identification in structural dynamics. Mechanical Systems and Signal Processing, 20(3), 505-592.

Klerk, D. d., Rixen, D. J., & Voormeeren, S. N. (2008). General framework for dynamic substructuring: History, review and classification of techniques. American Institute of Aeronautics and Astronautics Journal, 46(5), 1169-1181.

Kreutz, M., Trainotti, F., Gimpl, V., & Rixen, D. J. (2023). On the robust experimental multi-degree-of-freedom identification of bolted joints using frequency-based substructuring. Mechanical Systems and Signal Processing, 203, 110626.

Labbaci, B., Rahmani, O., Djermane, M., Boutchicha, D., Missoum, L., & Abdeldjebar, R. (2008). A study of the effect of the simulation of the boundary condition on dynamic response of composite structures. Journal of Applied Sciences, 8(11), 2098-2104.

Li, C., Jiang, Y., Qiao, R., & Miao, X. (2021). Modeling and parameters identification of the connection interface of bolted joints based on an improved micro-slip model. Mechanical Systems and Signal Processing, 153, 107514.

Liu, J., Ouyang, H., Peng, J., Zhang, C., Zhou, P., Ma, L., & Zhu, M. (2016). Experimental and numerical studies of bolted joints subjected to axial excitation. Wear, 346-347, 66-77.

Mahmoudi, A. E., Rixen, D. J., & Meyer, C. H. (2020). Comparison of different approaches to include connection elements into frequency-based substructuring. Experimental Techniques, 44(4), 425-433.

Maia, N. M. M., & Silva, J. M. M. (1997). Theoretical and experimental modal analysis. Research Studies Press.

Mathis, A. T., Balaji, N. N., Kuether, R. J., Brink, A. R., Brake, M. R. W., & Quinn, D. D. (2020). A review of damping models for structures with mechanical joints. Applied Mechanics Reviews, 72(4), 040802.

Mirza, W. I. I. W. I., Kyprianou, A., Silva, T. A. N., & Rani, M. N. A. (2024). Frequency based substructuring and coupling enhancement using estimated rotational frequency response functions. Experimental Techniques, 48(3), 423-437.

Mirza, W. I. I. W. I., Rani, M. N. A., Othman, M. H., Kasolang, S., & Yunus, M. A. (2016). Reduced order model for model updating of a jointed structure. Journal of Engineering and Applied Sciences, 11(11), 2383-2386.

https://doi.org/10.24191/jmeche.v22i3.5782

Mirza, W. I. I. W. I., Rani, M. N. A., Yunus, M. A., Ayub, M. A., Sani, M. S. M., & Zin, M. S. M. (2019). Frequency based substructuring for structure with double bolted joints: A case study. International Journal of Automotive and Mechanical Engineering, 16(1), 6188-6199.

Mohd Kahar, M. S. A., Wan Iskandar Mirza, W. I. I., Abdul Rani, M. N., & Yunus, M. A. (2024). Finite element modelling for the dynamic behaviour analysis of a structure with Hi-Lok fasteners. Journal of Mechanical Engineering, 21(3), 231-246.

Prandina, M., Mottershead, J. E., & Bonisoli, E. (2009). An assessment of damping identification methods. Journal of Sound and Vibration, 323(3-5), 662-676.

Ren, Y., & Beards, C. F. (1995). On substructure synthesis with FRF data. Journal of Sound and Vibration, 185(5), 845-866.

Sah, S. M., Thomsen, J. J., Brøns, M., Fidlin, A., & Tcherniak, D. (2018). Estimating bolt tightness using transverse natural frequencies. Journal of Sound and Vibration, 431, 137-149.

Shi, B., Luo, Z., Li, L., Li, Y., & Sun, K. (2024). Joint degradation and its effect on rotor vibration characteristics considering bolt assembly process. Mechanical Systems and Signal Processing, 211, 111208.

Sulaiman, M. S. A., Yunus, M. A., Abdul Rani, M. N., Mohd Saman, A., Mohamed, Z., & Aziz Shah, M. A. S. (2017). Characterisation of the dynamic characteristics of a complex jointed structure. MATEC Web of Conferences, 108, 12001.

Wang, L., & Yang, Z. (2011). Identification of boundary conditions of tapered beam-like structures using static flexibility measurements. Mechanical Systems and Signal Processing, 25(7), 2484-2500.

Yu, P., Li, L., Chen, G., & Yang, M. (2021). Dynamic modelling and vibration characteristics analysis for the bolted joint with spigot in the rotor system. Applied Mathematical Modelling, 94, 306-331.

Yunus, M. A., Aziz Shah, M. A. S., Abdul Rani, M. N., Wan Iskandar Mirza, W. I. I., & Kushairi, S. (2017). Experimental and finite element analysis of laser stitch welded structure. Journal of Mechanical Engineering, SI 4(3), 155-162.

Zhang, S., Devriendt, H., Belle, L. V., & Desmet, W. (2024). Substructuring-based parametric reduced-order modelling for structural dynamic predictions of bolted assemblies. Mechanical Systems and Signal Processing, 218, 111513.

https://doi.org/10.24191/jmeche.v22i3.5782